AGU PUBLICATIONS

Geophysical Research Letters

RESEARCH LETTER
10.1002/2017GL073938

Key Points:
- A new method that uses the granular porous media directly
- The developed method is used to generate granular media on various simulation grids
- The algorithm is applied on one complex sand example

Supporting Information:
- Supporting Information S1

Correspondence to:
P. Tahmasebi,
ptahmase@uwyo.edu

Citation:
Tahmasebi, P., M. Sahimi, and J. E. Andrade (2017), Image-based modeling of granular porous media, *Geophys. Res. Lett.*, *44*, 4738–4746, doi:10.1002/2017GL073938.

Received 2 MAR 2017
Accepted 27 APR 2017
Accepted article online 2 MAY 2017
Published online 21 MAY 2017

Image-based modeling of granular porous media

Pejman Tahmasebi[1,2], Muhammad Sahimi[3], and José E. Andrade[2]

[1]Department of Petroleum Engineering, University of Wyoming, Laramie, Wyoming, USA, [2]Division of Engineering and Applied Science, California Institute of Technology, Pasadena, California, USA, [3]Mork Family Department of Chemical Engineering and Materials Science, University of Southern California, Los Angeles, California, USA

Abstract We propose a new method of modeling granular media that utilizes a single two- or three-dimensional image and is formulated based on a Markov process. The process is mapped onto one that minimizes the difference between the image and a stochastic realization of the granular medium and utilizes a novel approach to remove possible unphysical discontinuities in the realization. Quantitative comparison between the morphological properties of the realizations and representative examples indicates excellent agreement.

1. Introduction

Granular porous media, represented by packings of particles of various shapes and sizes, are important to various fields of science and engineering, ranging from soil, oil and gas reservoirs, to civil and chemical engineering, mining, and agriculture [*Mehta*, 1994; *Cambou et al.*, 2009; *Sahimi*, 2011]. Such fascinating problems as formation of sand dunes [*Amarouchene et al.*, 2001; *Kroy et al.*, 2002] have to do with the formation of packing of sands. In addition, although such porous media consist of solid particles, they may behave like a fluid, which is why they are representative of what are sometimes called *collective systems*—those in which a small perturbation on one side affects the entire system. It is for such reasons that unconsolidated porous, or granular, media have been studied for decades.

The morphology of granular media is the most important factor in setting their fluid flow and transport properties. In addition, the shape of the particles and their chemical composition control the interparticle forces and, consequently, their macroscopic mechanical properties. Thus, accurate characterization and modeling of the morphology are critical to a wide variety of phenomena in which granularity plays a fundamental role. Although on the experimental side unconsolidated and granular media have been studied using a variety of techniques [*Cavarretta et al.*, 2010, and references therein], the modeling approaches used so far are not capable of comprehensive characterization of such porous media, when the particles do not have regular shapes.

Models of packing of particles may be divided into three broad groups. In one group are what we call the *object-based models*, which are those that model porous media as a collection of particles or objects, *regardless* of how they have been formed [*Torquato*, 2002; *Sahimi*, 2003, 2011]. In the earliest approach [*Cundall and Strack*, 1979] particles with relatively simple shapes, such as circles and spheres, were used [*Salot et al.*, 2009; *Katagiri et al.*, 2010; *Stahl and Konietzky*, 2011], for which the computations are straightforward, with their flow properties typically computed by the lattice Boltzmann method [*Pan et al.*, 2004], their diffusion and electrical conductivity by the random walk method [*Sahimi*, 2011], while the mechanical properties are studied by the discrete-element method (DEM) [*Cundall and Strack*, 1979]. The DEM is, however, accurate if the granular medium consists of particles that are not too complex. Packings with such particle shapes as ellipsoids [*Sherwood*, 1997; *Man et al.*, 2005; *Ng*, 2009], cylinders [*Pournin et al.*, 2005], polyhedra [*Tillemans and Herrmann*, 1995; *Lu and McDowell*, 2006; *Peña et al.*, 2007; *Azéma et al.*, 2009; *Galindo-Torres and Pedroso*, 2010; *Mollon and Zhao*, 2012], polyarcs [*Fu and Dafalias*, 2011], pentagons [*Azéma et al.*, 2007], rounded rectangles [*Boon et al.*, 2012], and cubes [*Malmir et al.*, 2016a, 2016b] have been studied.

In the second class of models of granular porous media are *process-based models* that are those that try to mimic the physical processes, such as sedimentation and weathering, which gave rise to their present state [*Roberts and Schwartz*, 1985; *Biswal et al.*, 1999, 2007]. They are, however, appropriate for consolidated porous media in which the particles have been somehow fused. Though accurate, the computational burden of such techniques is also high. Furthermore, a set of separate rules for each type of granular media with different formation process need to be defined that requires extensive calibrations.

The last group consists of the *statistical* methods by which various statistical properties, derived from either point data or an image, are extracted and used to generate stochastic realizations of the porous medium. Indicator simulation is one of the first methods that was developed for modeling of binary systems with high entropy (strong heterogeneity) [*Goovaerts*, 1997]. Similarly, sequential Gaussian simulation was developed for continuous properties, such as porosity and permeability [*Journel and Huijbregts*, 1978; *Deutsch and Journel*, 1998]. All of such methods are sequential algorithms in that the cells in the simulation grid are visited successively [*Adler et al.*, 1990; *Hilfer*, 2000, 2002; *Manwart et al.*, 2000; *Okabe and Blunt*, 2007; *Hyman and Winter*, 2014].

Recent progress in two- and three-dimensional (3-D) imaging provides the basis for the ultimate approach to accurate modeling of granular porous media. X-ray computed tomography, for example, provides valuable information about the spatial distribution and size of the particles [*Cavarretta et al.*, 2010], as well as the elastic strains under loading, void ratio in a shear band [*Alshibli and Hasan*, 2008], and the spatial movement of the particles [*Andò et al.*, 2012]. Several methods have been proposed to take advantage the 2-D/3-D images [*Garboczi*, 2002; *Andrade and Tu*, 2009; *Andrade et al.*, 2012; *Lim and Andrade*, 2014; *Tahmasebi et al.*, 2015a, 2015b, 2016a, 2016b]. It is also of interest to produce multiple realizations of any porous medium since, due to the cost and time limitations, one usually has only one or very few images.

The core idea in any modeling method is to incorporate the maximum amount of available information in the model. Clearly, 2-D/3-D images provide the highest amount of information, since they represent the particles as they exist in the sample [*Aste et al.*, 2005; *Saadatfar*, 2009; *Sufian et al.*, 2015; *Tahmasebi and Sahimi*, 2016a, 2016b]. A large number of images is required, however, if one is to study important characteristics of porous media, whereas due to their high cost and the time that they require, 3-D images cannot be acquired extensively. Typically, at most only a few 2-D/3-D images may be available, which are not sufficient for reliable predictions, if the current modeling approaches are used. Moreover, the images' size is usually very small, whereas one would like to generate much larger realizations of granular porous media. Due to lack of similarity between the data, however, most of the current methods generate discontinuity and artifacts when they build a model much larger than the image's original size.

In this Letter we propose a new method in which only a single 2-D or 3-D image I is used, which is a representative of the granular media's morphology. We show that the method extracts the maximum amount of information from the image and incorporates the existing complexity of granular porous medium. The extracted information is maximized because the image and its raw information are used, rather than using some low-order statistical descriptors that the traditional models use. This renders unnecessary any simplification of the morphology of the pore and particle phases in the medium. Furthermore, the particles are reconstructed together, and thus, the spatial interactions between them are implicitly taken into account. As we demonstrate below, unlike the previous techniques, the method that we describe in this Letter produces high-quality realizations that are close to the size of the systems encountered in practice.

2. The Approach

Consider a 2-D or 3-D image I of a granular porous medium. To generate a model for the medium, we develop a Markov algorithm that at each stage uses the previously constructed particles to compute the probability of occurrence of the next grain. It begins with a computational grid $\mathbf{G} = \{\varkappa_1, \varkappa_2, \ldots, \varkappa_N\}$, where N is the number of points in $\mathbf{G}$, each of which takes a single value $\varkappa_i$. The probability of having a specific value of a pixel (voxel in 3-D) is given by $p(\mathbf{Z}) = p(\varkappa_1)p(\varkappa_2|\varkappa_1)\ldots p(\varkappa_N|\mathbf{Z}_{\Phi_N})$, where $p(\varkappa_N|\mathbf{Z}_{\Phi_N}) = p(\varkappa_N|\varkappa_{N-1}, \ldots, \varkappa_2, \varkappa_1)$ is the conditional probability of $\varkappa_N$. Thus, by the Markov nature of the process one has write, $p(\mathbf{Z}) = \prod_{i=1}^{N} p(\varkappa_i|\mathbf{Z}_{\Phi_i})$. Furthermore, other conditional probabilities, such as those associated with some data ξ_i that must be honored, may also be included, so that,

$$p(\boldsymbol{Z}) = \prod_{i=1}^{N} p\left(\varkappa_i|\boldsymbol{Z}_{\Phi_i}, \boldsymbol{Z}_{\xi_i}\right), \tag{1}$$

which should be calculated for each single point visited in $\mathbf{G}$.

Thus, the algorithm begins from point z_1 in $\mathbf{G}$, samples I, picks at random one pixel (voxel), and attributes it to z_1. I is a binary image in which the indicator function $I(r) = 1$ or 0, if a point at r either belongs to a particle or is in the pore space, respectively. One then moves to z_2, calculates the conditional

probability $p(z_2|z_1)$, and picks a pixel with probability $p(z_2|z_1)$ to attribute it to z_2. As the number of the inserted points z_i increases, however, calculating the conditional probabilities becomes more time-consuming. For example, if $z_1 = 1$ ($\varkappa_1$ is in the particle phase), to insert $\varkappa_2$, we only have two possibilities, either $\varkappa_2 = 0$ or 1. Thus, we compute the probability of both configurations in I and pick the one with the higher probability, or draw a random number, distributed uniformly in (0,1), and decide which one to accept. If, for example, $\varkappa_2 = 1$, we identify all the neighboring points in I for which $\varkappa_1 = 0$ and $\varkappa_2 = 1$ and calculate the conditional probability that $\varkappa_3 = 0$ or 1. Thus, calculating the conditional probabilities becomes rapidly computationally prohibitive.

One may simplify the computations by recalling that the correlations in a Markov process decay exponentially fast. Thus, there are only two finite ranges r_x and r_y (and similarly three ranges in 3-D) over which one needs to compute the conditional probabilities. To calculate them, we compute the covariances $\gamma(x)$ and $\gamma(y)$. The distances r_x and r_y at which the $\gamma(x)$ and $\gamma(y)$ achieve constant values represent the desired ranges. But, even calculating the conditional probabilities over r_x and r_y is too time-consuming for a large image with millions of pixels.

It can be shown that modeling a disordered medium based on the conditional probability given by equation (1) is equivalent to minimizing a Euclidean distance $d^2 = \sum (D - I)^2$ between the input image I and a stochastically-sampled data $D(i,j)$ of size $r_x \times r_y$ centered at (i,j) in **G**. This decreases the computational burden significantly, but it is still not feasible when one deals with a large image. Thus, to further reduce the computations, one considers [*Tahmasebi and Sahimi*, 2012, 2013] overlap regions ***O*** of size $O_x \times O_y$ (and similarly in 3-D) between the neighboring blocks of **G** and minimizes the Euclidean distance between the data contained in ***O*** and the image I, reducing further the computations.

Therefore, the algorithm selects stochastically a sample from I, inserts it in a block D of **G**, and continues by visiting the blocks of **G** along a given path. Next, the Euclidean distances between the ***O*** regions and I are minimized. If any distance is less than a preset threshold, the corresponding sample is considered acceptable. Several of such candidate samples are generated, and one of which is selected randomly and inserted permanently in the corresponding block of **G**. The process continues until **G** is filled. To further reduce the computations, the image I is transferred to the frequency domain [*Duhamel and Vetterli*, 1990] using fast Fourier transformation (FFT). Thus, the FT of the 3-D image I, partitioned into cells of size $O_x \times O_y \times O_z$, is given by

$$\hat{\mathrm{I}}(\boldsymbol{\omega}) = \sum_{x=0}^{O_x-1} \sum_{y=0}^{O_y-1} \sum_{z=0}^{O_z-1} \mathbf{I}(x,y,z) \exp\left[2\pi \mathrm{i}\left(x\omega_x/\mathbf{O}_x + y\omega_y/\mathbf{O}_y + z\omega_z/\mathbf{O}_z\right)\right]. \tag{2}$$

Similarly, the data in the ***O*** regions are also transferred to the Fourier domain. The Euclidean distances are computed and minimized in that domain, and the results are inverted by inverse FFT. This reduces the computation time by a factor 10–20, but it is still not fast enough for generating very large realizations.

3. The Multiscale Approach

We next introduce a *multiscale approach* by which the computations are greatly reduced without losing accuracy. We first upscale the original image I into a few (typically three) increasingly coarser images. A bi-(tri)-cubic interpolation is used with continuous images in order to produce the coarser images. The interpolated value $v(x,y,z)$ in a coarse image is computed using n^3nearest-neighbor values at $\left(u_{x_i}, u_{y_j}, u_{z_k}\right)$ by $v(x,y,z) = \sum_{i=1}^{n} \sum_{j=1}^{n} \sum_{k=1}^{n} \alpha_{ijk} u_{x_i} u_{y_j} u_{z_k}$, where the $n^3 = 64$ coefficients α_{ijk} are determined based on the given data. In the case of a binary I, one utilizes a simple nearest-neighbor interpolation. The multiscale approach then utilizes the coarser images in the above algorithm. The location of an acceptable data sample in the coarsest image is selected and projected onto the next finer image, and a window for sampling the data is placed around the projected area, hence avoiding sampling the entire I. The projection and search are continued until a matching sample is identified in the original I. With the computations carried out in the Fourier space, the speed-up factor is 50–80, depending on the complexity of the original image, fast enough to make the method applicable to very large materials and media.

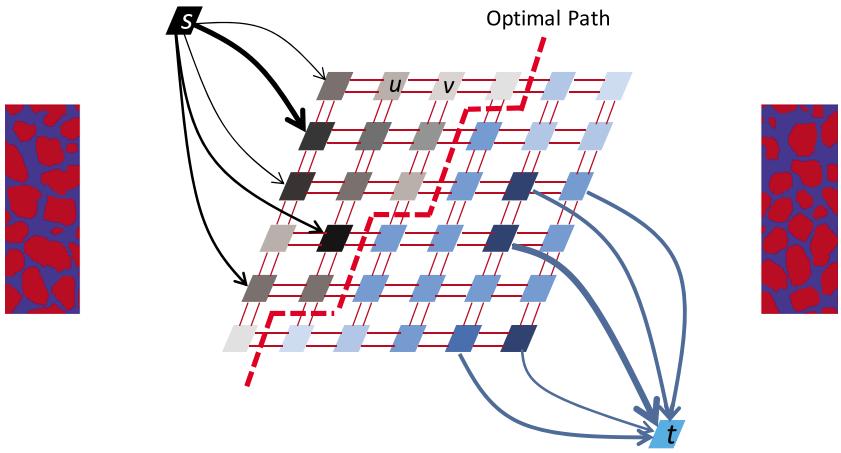

Figure 1. Two mismatched neighboring overlap regions and their representation by the graph in the middle. The optimal path matches the overlaps.

4. Removing the Unphysical Features

The multiscale algorithm produces very accurate results, if the particles' shapes are not too irregular. If, however, they have highly complex shapes, the algorithm produces discontinuities, or *patchiness*, in their spatial distribution. To alleviate the problem with patchiness, we use the graph theory that identifies an optimal path for matching various segments produced by the algorithm. In this method, the difference between the pixel (voxel) values in the corresponding neighboring $\boldsymbol{O}$ regions where the patchiness occurs is represented by a graph $\boldsymbol{G}_p$; see Figure 1. The nodes of $\boldsymbol{G}_p$ are either (i) *terminals*, representing sources **s** from which "flow" begins, and sinks **t** where the flow ends, and (ii) nonterminal nodes **P** that are in between the sinks and sources. Then, $\boldsymbol{G}_p = \{V, E\}$ consists of vertices $V = \boldsymbol{P} \cup \{\boldsymbol{s}, \boldsymbol{t}\}$ and the edges E. Two types of edges exist in the graph, namely, the *t-edges* $\{(\boldsymbol{s}, \boldsymbol{t}), (\boldsymbol{u}, \boldsymbol{t})\}$ and the *n edges* that connect, respectively, a nonterminal node in **P** with a terminal node, and two nonterminal nodes denoted by N. Two constraints are imposed on $f(u, v)$, the pixels (voxels) values at points (u, v) in $\boldsymbol{G}_p$, from a source toward a sink: (i) $f(u, v)$ should satisfy "mass" conservation law, $\forall v \in V \setminus \{s, t\} : \sum_{\{u\,:\,(u,\,v)\,\in\,E\}} f(u, v) =$,and (ii) antisymmetry relation, $\forall (u, v) \in V : f(u, v) = -f(v, u)$.

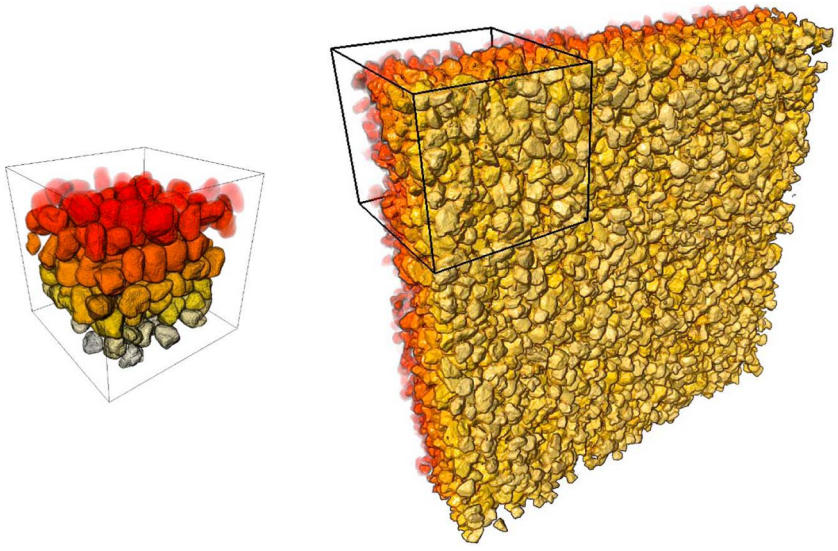

(a) (b)

Figure 2. (a) The image of a 3-D sand sample and (b) a much larger realization of it in which the cube shows the corresponding model for the original image.

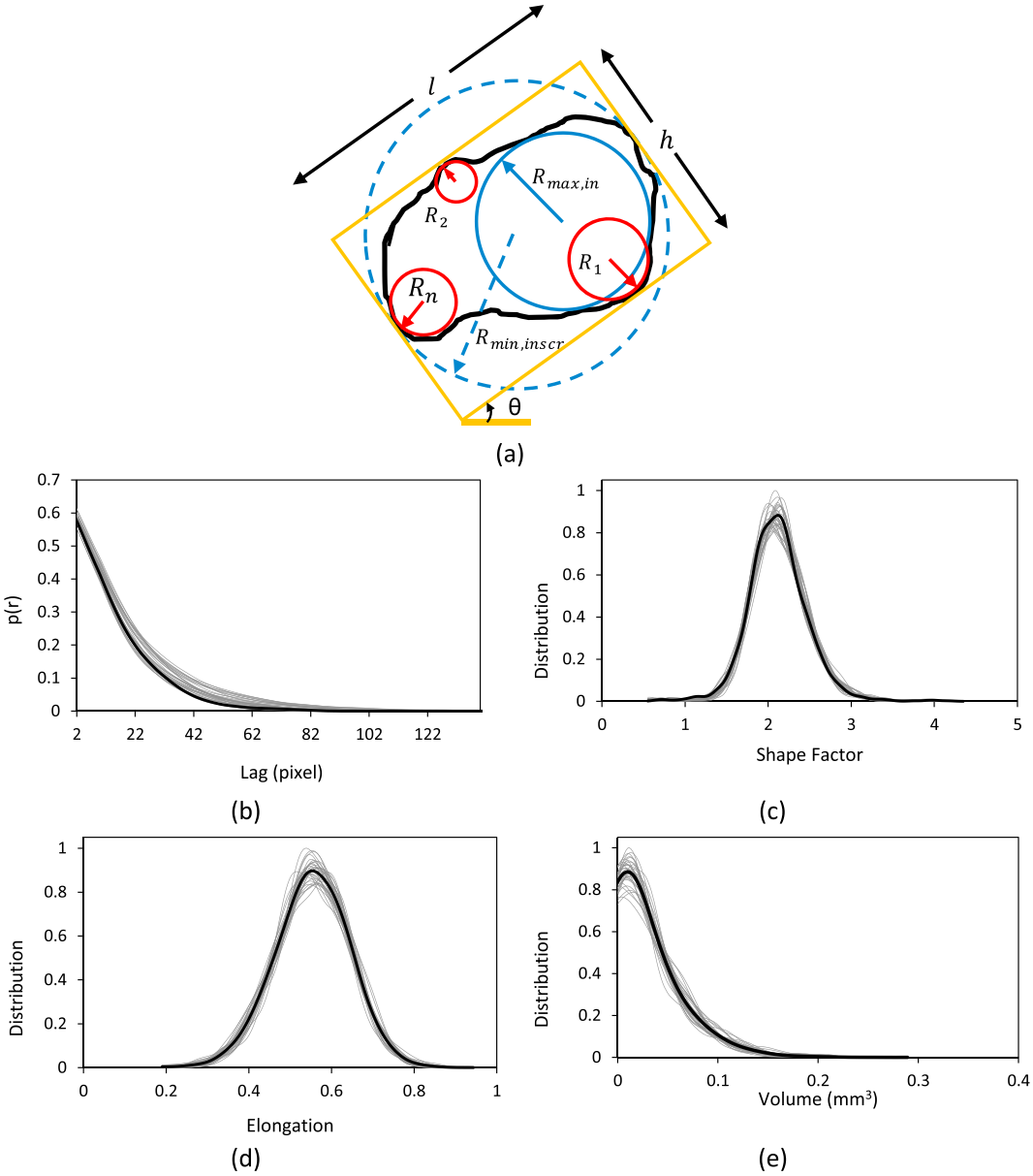

Figure 3. (a) Geometrical parameters of a particle. (b–e) Comparison of the morphological characteristics of sandstone of Figure 2 in terms of the distributions of the various properties is shown. $p(r)$ is the multiple-point connectivity function. The black curves indicate the results for the original image.

The optimal path is one that minimizes the overall flow, i.e., the difference between two neighboring patterns when they are interlocked at their joint interface, and is expressed as two subsets S and T, derived from a source **s** and a target sink **t**. The "cost" C of the path to be minimized is $C(S,T) = \sum_{u \in S}\sum_{v \in T} C(u,v)$. The minimization is solved [*Boykov et al.*, 2001] as a "fluid flow" model in which the optimal path allows a minimum amount of "fluid" passing from **s** to **t** with $|f| = \sum_{v \in V} f(s,v)$, and $f(\mathcal{S},\mathcal{T}) = \sum_{u \in \mathcal{S}}\sum_{v \in \mathcal{T}} f(u,v)$. As a fraction of the total computation time, the CPU time for identifying the optimal path is negligible but solves the problem of patchiness.

5. Results and Discussions

We present two examples. One is a complex $300 \times 300 \times 280$ sand material with a resolution of 3.1 μm, shown in Figure 2a for which 35 stochastic realizations of size $10^3 \times 10^3 \times 300$ were generated, one of which is shown

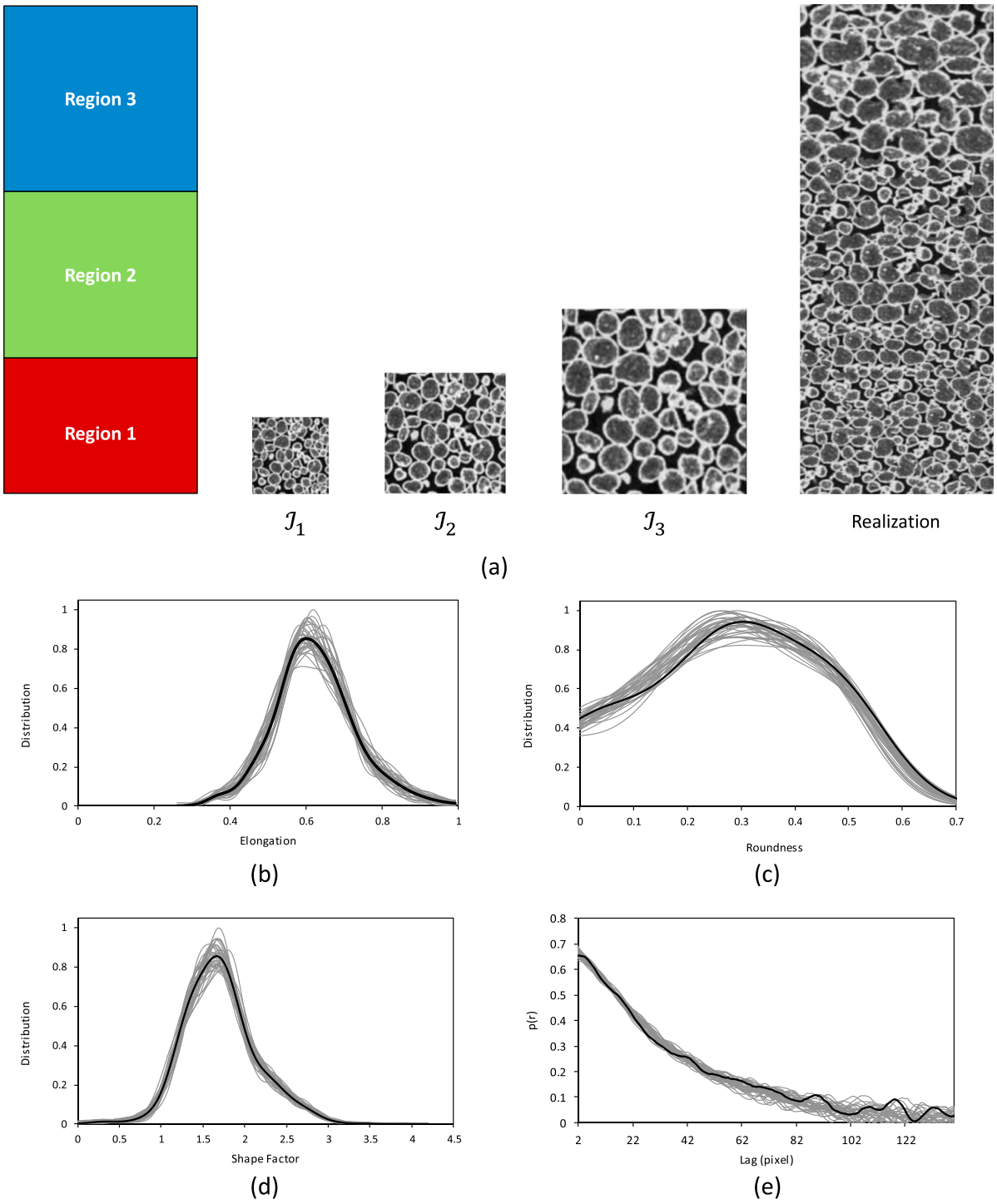

Figure 4. Incorporating scale-dependent heterogeneity using three regions, corresponding to three scales. Also shown is the comparison of the properties of the grains in the reconstructed realizations and the original image.

in Figure 2b. Each realization took seven CPU minutes to generate. To make a quantitative test of the accuracy, consider an irregular particle shown in Figure 3a and place a rectangle around it, subject to the condition that the angle θ shown in the figure is minimum. Then, four quantities were computed for the 35 realizations and compared with the same calculated for the image. (i) The first quantity is multiple-point connectivity (MPC) function, the probability of having a sequence of *m* connected points in a given

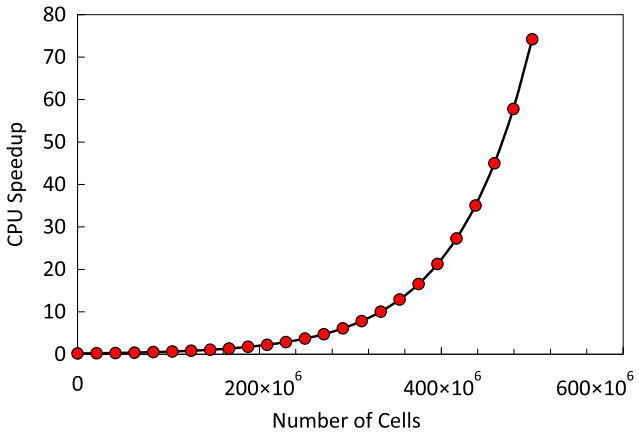

Figure 5. Dependence of the speed-up in the computation time on the number of grid cells in the 3-D model.

direction and phase (particle or void), defined by $p(\mathbf{h};m) = \text{Prob}\{I(\mathbf{u}) = 1, I(\mathbf{u}+\mathbf{h}) = 1, \ldots, I(\mathbf{u}+m\mathbf{h})\} = 1$, where $\mathbf{h}$ is a vector along which the probability $p(\mathbf{h};m)$ is calculated. $p(\mathbf{h};m)$ represents the frequency of the grains touching each other. The results are shown in Figure 3b for $m = 100$. The average error of the reconstructed realizations relative to the original image is 1.28% with a variance of 6.65×10^{-9}. (ii) The second is *shape factor*, defined by $F = (\text{Crofton perimeter})^2/(4\pi \times \text{area})$, where the Crofton perimeter (length) is a geometrical characteristic that relates the length of a curve (perimeter) to the average number of times that a random line intersects it [*Mecke*, 1979]. The resulting distribution of the shape factors is shown in Figure 3c. The average error of the realizations is 7.78% with a variance of 0.05. (iii) The *elongation* is defined by $E = h/l$. The computed distribution is shown in Figure 3d. The average error of the realizations is 2.72% with a variance of 1.8×10^{-4}. (iv) The volume distribution of the grains is shown in Figure 3e, with an average error of 1.3% and a variance of 5.52×10^{-8}. All the computed properties of the realizations agree excellently with those for the original system.

We also computed the Darcy permeability K of the original image by solving the Stokes' equation and using Darcy's law (the details are given in Text SI) [*Karimpouli and Tahmasebi*, 2016]. The result is $K = 810$ mD, which should be compared with the computed average permeability of the 35 realizations, $K = 798$ mD. To compare the accuracy of the flow calculations with that of an efficient alternative method, we also used the method of single normal equation simulation (SNESIM) algorithm [*Strebelle*, 2002], which is considered to be the best alternative method for modeling of categorical porous media [*Journel and Zhang*, 2006]. The SNESIM algorithm was used to reconstruct the granular medium using the 3-D image in Figure 2a, and its permeability was computed. The flow simulation was carried out on multiple 3-D realizations of size $300 \times 300 \times 300$ voxels. Since the SNESIM algorithm is computationally very expensive, the size of the computational grid for the flow simulation was the same as that of the reconstructed realizations (the much larger system of Figure 2b was used in the flow simulation in the realizations generated by our algorithm).The result is $K = 3587$ mD, more than 4 times the actual value, $K = 810$ mD. Note that with the SNESIM algorithm the CPU time for producing a single realization was 10 h. Thus, very large realizations, such as the one shown in Figure 2b, cannot even be generated by the SNESIM algorithm. The details of the flow simulation along with a comparison of the spatial distributions of the velocity and pressure fields in the original image, a realization generated by the proposed algorithm, and one by the SNESIM method are given in the Text SI.

We emphasize that the proposed algorithm has no limitation in terms of the number of input images that it can utilize. It incorporates the heterogeneity by two methods: (i) through an auxiliary data set and/or (ii) multiple images, if available, representing the heterogeneities of multiple regions of the material. The second example, shown in Figure 4, incorporates the heterogeneities at multiple length scales, representing a nonstationary medium. The comparison between the properties of the original sample and averages over multiple realizations of it is shown in Figure 4. The mean errors (in percentage) and variances for the MPC function, elongation, shape factor, and roundness are, respectively, $(0.95, 1.76 \times 10^{-5})$, $(1.27, 4.24 \times 10^{-5})$, $(2.89, 4.25 \times 10^{-6})$, and $(1.94, 2.21 \times 10^{-8})$. The roundness is defined by $R = \frac{\sum_i^M R_i}{N.R_{\max-\text{in}}}$, where R_i is an estimate of the radius of circle (sphere)i, M of which approximate the particles' corners, and describes the texture of the surface of the particles and their sharpness and edges.

The efficiency of the proposed method is quantified by comparing the speed-up, relative to the original Markov formulation, in the computation time as a function of the size of the simulation grid. The results

are shown in Figure 5. The combined FFT and multiscale approaches reduce the CPU time by up to nearly 2 orders of magnitude and increase rapidly with the size of the simulation grid.

6. Summary

Accurate generation of models of granular porous media, and in particular their particles' shapes, have been long-standing problems. Past modeling approaches require analyzing a very large number of images, which is not feasible. The approach proposed in this Letter generates accurate models of granular materials and quantifies the uncertainties and range of the variability. The method is based on utilizing a single 2-D/3-D image. The raw image is used in a stochastic Markovian framework, together with a graph-theoretical approach that generates. While the previous methods are unable to model complex granular media or require days or months of computations to produce large and accurate realizations, the proposed method accomplishes the task and is capable of generating models with hundreds of millions of simulation grid cells by an affordable computation time.

Acknowledgments
The first author would like to thank the financial support from the University of Wyoming for this research. Work at USC was supported in part by the Petroleum Research Fund, administered by the American Chemical Society. All the data and digital content in this manuscript can be accessed by sending an e-mail to P.T. at ptahmase@uwyo.edu. We thank the Editor and reviewers for their constructive comments.

References

Adler, P. M., C. G. Jacquin, and J. A. Quiblier (1990), Flow in simulated porous media, *Int. J. Multiphase Flow*, *16*(4), 691–712, doi:10.1016/0301-9322(90)90025-E.

Alshibli, K. A., and A. Hasan (2008), Spatial variation of void ratio and shear band thickness in sand using X-ray computed tomography, *Géotechnique*, *58*(4), 249–257, doi:10.1680/geot.2008.58.4.249.

Amarouchene, Y., J. F. Boudet, and H. Kellay (2001), Dynamic sand dunes, *Phys. Rev. Lett.*, *86*(19), 4286–4289, doi:10.1103/PhysRevLett.86.4286.

Andò, E., S. A. Hall, G. Viggiani, J. Desrues, and P. Bésuelle (2012), Grain-scale experimental investigation of localised deformation in sand: A discrete particle tracking approach, *Acta Geotech.*, *7*(1), 1–13, doi:10.1007/s11440-011-0151-6.

Andrade, J. E., and X. Tu (2009), Multiscale framework for behavior prediction in granular media, *Mech. Mater.*, *41*(6), 652–669, doi:10.1016/j.mechmat.2008.12.005.

Andrade, J. E., K.-W. Lim, C. F. Avila, and I. Vlahinić (2012), Granular element method for computational particle mechanics, *Comput. Methods Appl. Mech. Eng.*, *241*, 262–274, doi:10.1016/j.cma.2012.06.012.

Aste, T., M. Saadatfar, and T. Senden (2005), Geometrical structure of disordered sphere packings, *Phys. Rev. E*, *71*(6), 61302), doi:10.1103/PhysRevE.71.061302.

Azéma, E., F. Radjaï, R. Peyroux, and G. Saussine (2007), Force transmission in a packing of pentagonal particles, *Phys. Rev. E*, *76*(1), 11301), doi:10.1103/PhysRevE.76.011301.

Azéma, E., F. Radjai, and G. Saussine (2009), Quasistatic rheology, force transmission and fabric properties of a packing of irregular polyhedral particles, *Mech. Mater.*, *41*(6), 729–741, doi:10.1016/j.mechmat.2009.01.021.

Biswal, B., C. Manwart, R. Hilfer, S. Bakke, and P. E. Øren (1999), Quantitative analysis of experimental and synthetic microstructures for sedimentary rock, *Phys. A Stat. Mech. Appl.*, *273*(3), 452–475, doi:10.1016/S0378-4371(99)00248-4.

Biswal, B., P.-E. Øren, R. J. Held, S. Bakke, and R. Hilfer (2007), Stochastic multiscale model for carbonate rocks, *Phys. Rev. E*, *75*(6), 61303, doi:10.1103/PhysRevE.75.061303.

Boon, C. W., G. T. Houlsby, and S. Utili (2012), A new algorithm for contact detection between convex polygonal and polyhedral particles in the discrete element method, *Comput. Geotech.*, *44*, 73–82, doi:10.1016/j.compgeo.2012.03.012.

Boykov, Y., O. Veksler, and R. Zabih (2001), Fast approximate energy minimization via graph cuts, *IEEE Trans. Pattern Anal. Mach. Intell.*, *23*(11), 1222–1239, doi:10.1109/34.969114.

Cambou, B., M. Jean, and F. Radja (Eds.) (2009), *Micromechanics of Granular Materials*, pp. 149-315, ISTE, London, U. K.

Cavarretta, I., M. Coop, and C. O'Sullivan (2010), The influence of particle characteristics on the behaviour of coarse grained soils, *Géotechnique*, *60*(6), 413–423, doi:10.1680/geot.2010.60.6.413.

Cundall, P. A., and O. D. L. Strack (1979), Development of constitutive laws for soil using the distinct element method, *SAE Prepr.*, *1*, 289–298.

Deutsch, C. V., and A. G. Journel (1998), *GSLIB: Geostatistical Software Library and User's Guide*, 2nd ed., Oxford Univ. Press, New York.

Duhamel, P., and M. Vetterli (1990), Fast Fourier transforms: A tutorial review and a state of the art, *Signal Process.*, *19*(4), 259–299, doi:10.1016/0165-1684(90)90158-U.

Fu, P., and Y. F. Dafalias (2011), Fabric evolution within shear bands of granular materials and its relation to critical state theory, *Int. J. Numer. Anal. Methods Geomech.*, *35*(18), 1918–1948, doi:10.1002/nag.988.

Galindo-Torres, S. A., and D. M. Pedroso (2010), Molecular dynamics simulations of complex-shaped particles using Voronoi-based spheropolyhedra, *Phys. Rev. E*, *81*(6), 61303), doi:10.1103/PhysRevE.81.061303.

Garboczi, E. J. (2002), Three-dimensional mathematical analysis of particle shape using X-ray tomography and spherical harmonics: Application to aggregates used in concrete, *Cem. Concr. Res.*, *32*(10), 1621–1638, doi:10.1016/S0008-8846(02)00836-0.

Goovaerts, P. (1997), *Geostatistics for Natural Resources Evaluation*, pp. 393–402, Oxford Univ. Press on Demand, New York.

Hilfer, R. (2000), Local porosity theory and stochastic reconstruction for porous media, in *Statistical Physics and Spatial Statistics*, pp. 203–241, Springer, Berlin.

Hilfer, R. (2002), Review on scale dependent characterization of the microstructure of porous media, *Transp. Porous Media*, *46*(2/3), 373–390, doi:10.1023/A:1015014302642.

Hyman, J. D., and C. L. Winter (2014), Stochastic generation of explicit pore structures by thresholding Gaussian random fields, *J. Comput. Phys.*, *277*, 16–31, doi:10.1016/j.jcp.2014.07.046.

Journel, A., and T. Zhang (2006), The necessity of a multiple-point prior model, *Math. Geol.*, *38*(5), 591–610.

Journel, A. G., and C. J. Huijbregts (1978), *Mining Geostatistics*, pp. 491–554, Academic Press, London, U. K.

Katagiri, J., T. Matsushima, and Y. Yamada (2010), Simple shear simulation of 3D irregularly-shaped particles by image-based DEM, *Granul. Matter*, *12*(5), 491–497, doi:10.1007/s10035-010-0207-6.

Karimpouli, S., and P. Tahmasebi (2016), Conditional reconstruction: An alternative strategy in digital rock physics, *Geophysics*, *81*(4), D465–D477, doi:10.1190/geo2015-0260.1.
Kroy, K., G. Sauermann, and H. J. Herrmann (2002), Minimal model for sand dunes, *Phys. Rev. Lett.*, *88*(5), 543,011–543,014, doi:10.1103/PhysRevLett.88.054301.
Lim, K.-W., and J. E. Andrade (2014), Granular element method for three-dimensional discrete element calculations, *Int. J. Numer. Anal. Methods Geomech.*, *38*(2), 167–188, doi:10.1002/nag.2203.
Lu, M., and G. R. McDowell (2006), The importance of modelling ballast particle shape in the discrete element method, *Granul. Matter*, *9*(1–2), 69–80, doi:10.1007/s10035-006-0021-3.
Malmir, H., M. Sahimi, and M. R. R. Tabar (2016a), Microstructural characterization of random packings of cubic particles, *Sci. Rep.*, *6*, 35,024, doi:10.1038/srep35024.
Malmir, H., M. Sahimi, and M. R. R. Tabar (2016b), Packing of nonoverlapping cubic particles: Computational algorithms and microstructural characteristics, *Phys. Rev. E*, *94*(6), 62901, doi:10.1103/PhysRevE.94.062901.
Man, W., A. Donev, F. H. Stillinger, M. T. Sullivan, W. B. Russel, D. Heeger, S. Inati, S. Torquato, and P. M. Chaikin (2005), Experiments on random packings of ellipsoids, *Phys. Rev. Lett.*, *94*(19), 198001, doi:10.1103/PhysRevLett.94.198001.
Manwart, C., S. Torquato, and R. Hilfer (2000), Stochastic reconstruction of sandstones, *Phys. Rev. E*, *62*(1), 893–899, doi:10.1103/PhysRevE.62.893.
Mecke, J. (1979), Santaló, L. A., Integral geometry and geometric probability (Encyclopedia of mathematics and its applications) 1. London-Amsterdam-don Mills-Sydney-Tokyo, Addison-Wesley publishing company 1976. XVII, 404 S., $ 17.50, *ZAMM-Z. Angew. Math. Mech.*, *59*(6), 286–286, doi:10.1002/zamm.19790590633.
Mehta, A. (Ed.) (1994), *Granular Matter*, pp. 18–26, Springer, New York.
Mollon, G., and J. Zhao (2012), Fourier–Voronoi-based generation of realistic samples for discrete modelling of granular materials, *Granul. Matter*, *14*(5), 621–638, doi:10.1007/s10035-012-0356-x.
Ng, T.-T. (2009), Particle shape effect on macro- and micro-behaviors of monodisperse ellipsoids, *Int. J. Numer. Anal. Methods Geomech.*, *33*(4), 511–527, doi:10.1002/nag.732.
Okabe, H., and M. J. Blunt (2007), Pore space reconstruction of vuggy carbonates using microtomography and multiple-point statistics, *Water Resour. Res.*, *43*, W12S02, doi:10.1029/2006WR005680.
Pan, C., M. Hilpert, and C. T. Miller (2004), Lattice-Boltzmann simulation of two-phase flow in porous media, *Water Resour. Res.*, *40*, W01501, doi:10.1029/2003WR002120.
Peña, A. A., R. García-Rojo, and H. J. Herrmann (2007), Influence of particle shape on sheared dense granular media, *Granul. Matter*, *9*(3–4), 279–291, doi:10.1007/s10035-007-0038-2.
Pournin, L., M. Weber, M. Tsukahara, J.-A. Ferrez, M. Ramaioli, and T. M. Liebling (2005), Three-dimensional distinct element simulation of spherocylinder crystallization, *Granul. Matter*, *7*(2–3), 119–126, doi:10.1007/s10035-004-0188-4.
Roberts, J. N., and L. M. Schwartz (1985), Grain consolidation and electrical conductivity in porous media, *Phys. Rev. B*, *31*(9), 5990–5997, doi:10.1103/PhysRevB.31.5990.
Saadatfar, M. (2009), Computer simulation of granular materials, *Comput. Sci. Eng.*, *11*(1), 66–74, doi:10.1109/MCSE.2009.4.
Sahimi, M. (2003), *Heterogeneous Materials I*, pp. 61–107, Springer, New York.
Sahimi, M. (2011), *Flow and Transport in Porous Media and Fractured Rock*, pp. 186–204, Wiley-VCH, Weinheim, Germany.
Salot, C., P. Gotteland, and P. Villard (2009), Influence of relative density on granular materials behavior: DEM simulations of triaxial tests, *Granul. Matter*, *11*(4), 221–236, doi:10.1007/s10035-009-0138-2.
Sherwood, J. D. (1997), Packing of spheroids in three-dimensional space by random sequential addition, *J. Phys. A: Math. Gen.*, *30*(24), L839–L843, doi:10.1088/0305-4470/30/24/004.
Stahl, M., and H. Konietzky (2011), Discrete element simulation of ballast and gravel under special consideration of grain-shape, grain-size and relative density, *Granul. Matter*, *13*(4), 417–428, doi:10.1007/s10035-010-0239-y.
Strebelle, S. (2002), Conditional simulation of complex geological structures using multiple-point statistics, *Math. Geol.*, *34*(1), 1–21.
Sufian, A., A. R. Russell, A. J. Whittle, and M. Saadatfar (2015), Pore shapes, volume distribution and orientations in monodisperse granular assemblies, *Granul. Matter*, *17*(6), 727–742, doi:10.1007/s10035-015-0590-0.
Tahmasebi, P., and M. Sahimi (2012), Reconstruction of three-dimensional porous media using a single thin section, *Phys. Rev. E: Stat. Nonlinear Soft Matter Phys.*, *85*(6), 1–13, doi:10.1103/PhysRevE.85.066709.
Tahmasebi, P., and M. Sahimi (2013), Cross-correlation function for accurate reconstruction of heterogeneous media, *Phys. Rev. Lett.*, *110*(7).
Tahmasebi, P., and M. Sahimi (2016a), Enhancing multiple-point geostatistical modeling: 1. Graph theory and pattern adjustment, *Water Resour. Res.*, *52*(3), 2074–2098, doi:10.1002/2015WR017806.
Tahmasebi, P., and M. Sahimi (2016b), Enhancing multiple-point geostatistical modeling: 2. Iterative simulation and multiple distance function, *Water Resour. Res.*, *52*(3), 2099–2122, doi:10.1002/2015WR017807.
Tahmasebi, P., F. Javadpour, and M. Sahimi (2015a), Multiscale and multiresolution modeling of shales and their flow and morphological properties, *Sci. Rep.*, *5*, 16373, doi:10.1038/srep16373.
Tahmasebi, P., F. Javadpour, and M. Sahimi (2015b), Three-Dimensional Stochastic Characterization of Shale SEM Images, *Transp. Porous Media*, *110*(3), 521–531, doi:10.1007/s11242-015-0570-1.
Tahmasebi, P., F. Javadpour, M. Sahimi, and M. Piri (2016a), Multiscale study for stochastic characterization of shale samples, *Adv. Water Resour.*, *89*, 91–103, doi:10.1016/j.advwatres.2016.01.008.
Tahmasebi, P., M. Sahimi, A. H. Kohanpur, and A. Valocchi (2016b), Pore-scale simulation of flow of CO2 and brine in reconstructed and actual 3D rock cores, *J. Pet. Sci. Eng.*, doi:10.1016/j.petrol.2016.12.031.
Tillemans, H.-J., and H. J. Herrmann (1995), Simulating deformations of granular solids under shear, *Phys. A Stat. Mech. Appl.*, *217*(3–4), 261–288, doi:10.1016/0378-4371(95)00111-J.
Torquato, S. (2002), *Random Heterogeneous Materials*, Interdisciplinary Applied Mathematics, pp. 269–302, Springer, New York.